

# Mountain building in the Nepal Himalaya: Thermal and kinematic model

L. Bollinger <sup>a,\*</sup>, P. Henry <sup>b</sup>, J.P. Avouac <sup>c</sup>

<sup>a</sup> *Laboratoire de Détection et de Géophysique CEA, BP12, Bruyères-le-Châtel, 91680, France*

<sup>b</sup> *CEREGE, Collège de France Europole de l'Arbois, BP 80-13545 Aix en Provence, France*

<sup>c</sup> *Tectonics Observatory, California Institute of Technology Pasadena, CA 91125, USA*

Received 27 June 2005; received in revised form 24 December 2005; accepted 23 January 2006

Available online 10 March 2006

Editor: V. Courtillot

## Abstract

We model crustal deformation and the resulting thermal structure across the Nepal Himalaya, assuming that, since 20Ma, shortening across the range has been primarily taken up by slip along a single thrust fault, the Main Himalayan Thrust (MHT) Fault, and that the growth of the Himalayan wedge has resulted mainly from underplating and to the development of a duplex at midcrustal depth. We show that this process can account for the inverse thermal metamorphic gradient documented throughout the Lesser Himalaya (LH), the discontinuity of peak metamorphic temperatures across the MCT, as well as the distribution of age of exhumation across the range. This study suggests that the metamorphic evolution of the range over about the last 20 million years is compatible with the kinematics of recent crustal deformation deduced from morphotectonic and geodetic studies.

© 2006 Elsevier B.V. All rights reserved.

*Keywords:* thermal model; temperature-time paths; inverted metamorphism; underplating; Himalayan orogen; Nepal Himalaya; Lesser Himalaya; Main Central Thrust; Main Himalayan Thrust; crustal tectonics

## 1. Introduction

Although continental collision belts are often pictured as zones of complex deformation, geophysical studies of the Himalayas lead to a simple picture with a single major shear zone (the MHT, for Main Himalayan Thrust), along which the Indian crust is subducted beneath the southern edge of Tibet [e.g., [1]]. The similarity between the slip rate along the MHT inferred from geomorphic studies of the Main Frontal Thrust at the front of the range [2], and the convergence rate across the Himalaya estimated from GPS measurements

[3,4] suggested that recent deformation in the Himalaya requires negligible internal shortening of the Himalayan wedge. Over the longer geological term, the Main Central Thrust fault, the major shear zone separating the High Himalayan Crystallines (HHC) from the Lesser Himalayan Series (LH), is thought to be the major thrust fault which has contributed to the formation of the Himalaya. Cooling ages and geomorphic considerations have been taken to suggest that the MCT zone was activated in the early Miocene [5] and may have been reactivated as an out of sequence thrust in the Pliocene [6] and may even still be active [7].

Studies in petrology and geochronology often aim at constraining *PTt* paths, which may then be reproduced by numerical models [e.g. [8] and references therein].

\* Corresponding author.

E-mail address: [laurent.bollinger@cea.fr](mailto:laurent.bollinger@cea.fr) (L. Bollinger).

Such models are generally not unique because precise constraints on the geometry and kinematics are, at best, available for the present day. Difficulties also arise from coupling between the temperature field and the deformation field. However, because of thermal diffusion, sudden changes of kinematics only cause progressive changes of the temperature field. In the Himalayas, peak metamorphic conditions recorded in the HHC and the MCT zone [e.g. [5,9]] appear compatible with the present day temperature field, as indicated by geophysical surveys and modeling studies [10–12]. This suggests that the temperature field in the Himalayas has been nearly steady-state over the last 20 Ma (within 100°C in the hottest and deepest parts of the model) [12]. However, the set of parameters and boundary conditions which fit these constraints is not uniquely determined because trade offs are involved, for example, between basal heat flow, radiogenic heat generation, and shear heating [12,13].

The spatial distribution of thermobarometric and thermo-chronological data is also important information, but their inclusion as modeling constraints require taking into account syn- and post-metamorphic deformation.

It is now understood that the inverted isograds in the MCT zone cannot only result from the ‘iron effect’ as a hotter hangingwall overthrusts a cooler footwall [e.g.: [14,15]], even combined with shear heating [16], but that some amount of syn- or post-metamorphic shearing is needed [17–19]. In the ductile realm, HHC exhumation between coeval normal and thrust sense shear zones (respectively, the Southern Tibetan Detachment System (STDS) and the MCT 20 Myr ago), has been modelled with the midcrustal channel flow concept [e.g. [20,21]]. However, the applicability of this model to the later evolution (post-15 Ma) of the frontal (and mostly brittle) part of the Himalayan wedge may be questioned.

Recently, the geological understanding of the frontal part of the range has been augmented with tectonic scenarios for the accretion of the Lesser Himalayas involving a migrating duplex system [22,23]. Observations within the MCT zone also imply transfer of material from the lower to the upper plate [24,25]. Dense thermometric and thermochronological profiles at the front of the range (Fig. 1A and B) were acquired through the crystalline klippe and the underlying Lesser

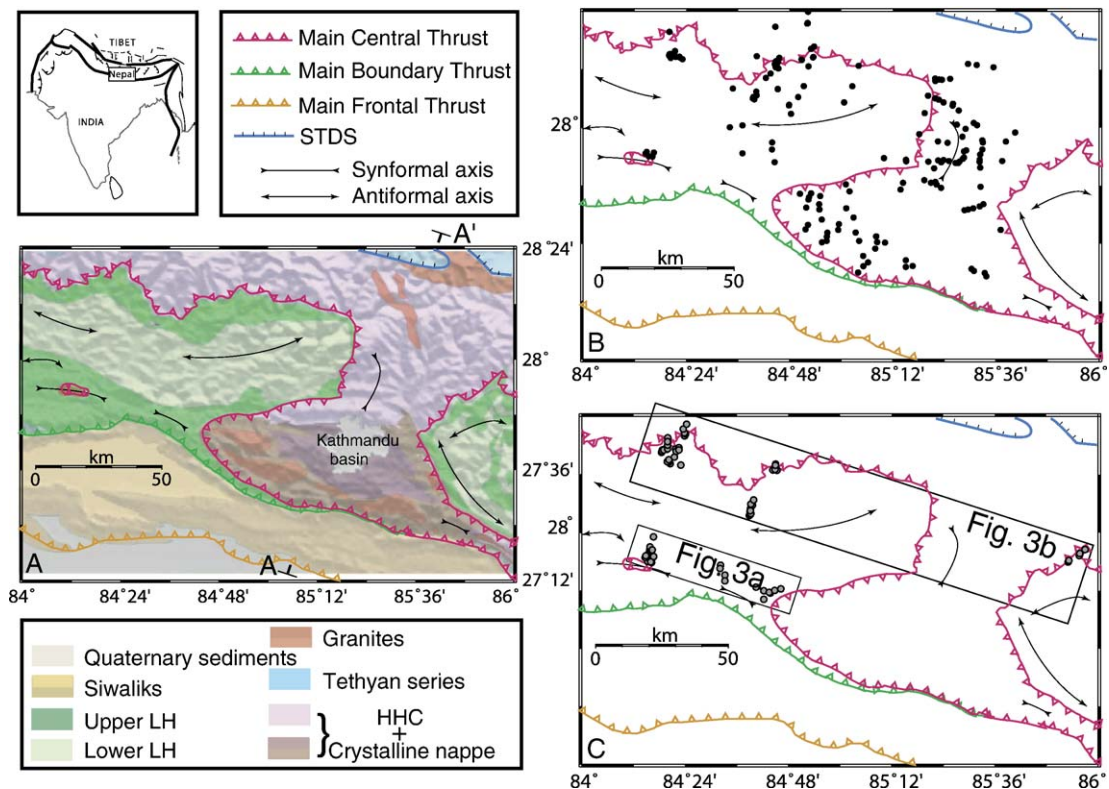


Fig. 1. Simplified geologic map with location of (A) thermochronological data [24,27,36,39,51–53] and [Copeland pers. comm., 1999] and (B) thermometric [24–27] data. AA' show location of section in Fig. 2. Boxes 3A and 3B show the location of the data in Fig. 3A and B, respectively. MCT: Main Central Thrust fault. MBT: Main Boundary Thrust fault. MFT: Main Frontal Thrust fault.

Himalayas [e.g. [26,27]]. These additional datasets provide appropriate constraints for kinematic and thermal models of the MCT zone evolution and Lesser Himalayas accretion. The model we here consider is derived from simple sliding block models [11,12,16]. The main improvement is that a flux of underplating, variable in time, is assigned to a window on the sliding surface. This window is located over the transition from the brittle part to the ductile part of the MHT and is assumed fixed with respect to the front of the range. Within this framework, we show that the muscovite closure age gradient in the HHC can be interpreted as a kinematic constraint on the rate of overthrusting and that the peak temperature gradients in the MCT zone and Lesser Himalayas relates to the flux of underthrusting. Extrapolating the current geometry and kinematics of the Himalayas over the last 20Ma without even considering episodic MCT reactivation may be consid-

ered as a far-fetched idea. Yet the model we present reproduces essential features in the data set. To us, this suggests that some invariant pattern of uplift and erosion, possibly related to the mechanical properties of the Main Himalayan Thrust, is acting on the Himalayas.

## 2. Tectonic framework

### 2.1. Structure

Geophysical and structural studies of the Himalayas suggest that all the major thrust faults in the Nepal Himalaya, including the Main Frontal thrust fault (MFT), the Main Boundary Thrust fault (MBT) and the Main Central Thrust fault (MCT) sole at depth into a single major shear zone, the Main Himalayan Thrust (MHT), along which the Indian crust is thrust under the

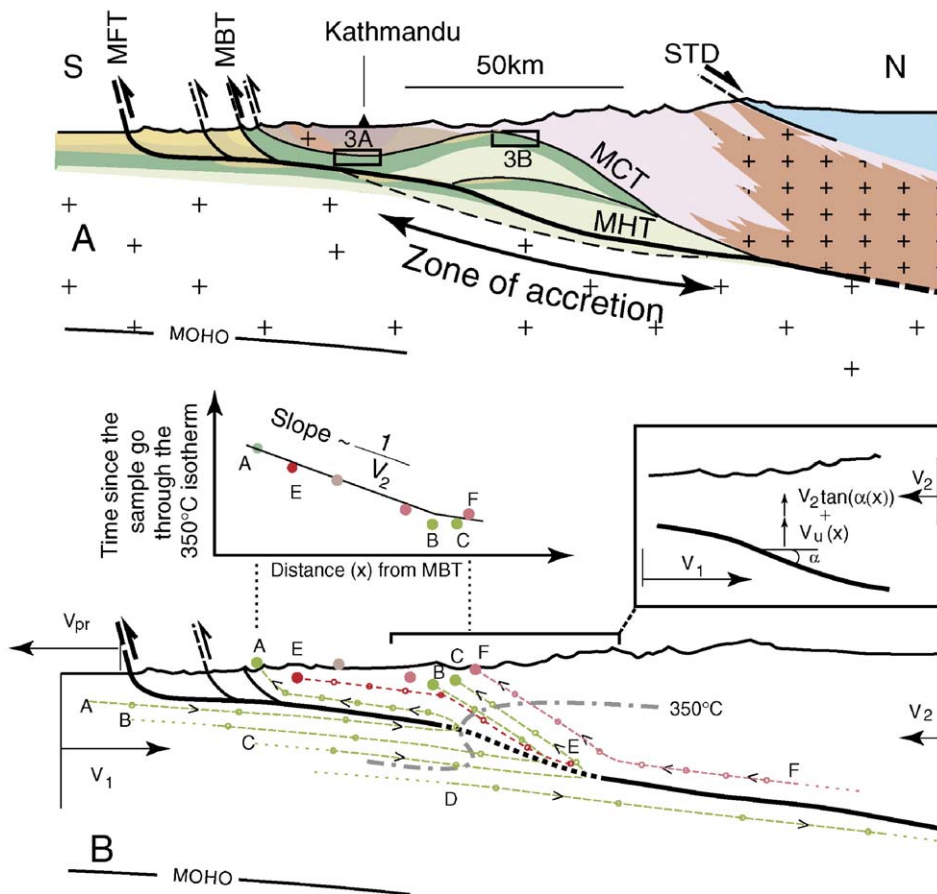


Fig. 2. A—Simplified N18E section across the Himalaya of Central Nepal. See Fig. 1B for location of section. Boxes A and B show the projected structural location for the sections in Fig. 3 where the inverse metamorphic thermal gradient was documented. B—Particle paths in a continuous model of accretion. The reference frame is the active thrust fault (the equivalent of the basal thrust fault connecting the MFT and the MHT in the present structure as shown in A). The dots show positions of particles for 3Myr time intervals.  $V_1$  and  $V_2$  are, respectively, the under and overthrusting velocities,  $V_{pr}$ , the sediment progradation velocity.

southern edge of Tibet [e.g., [1,10]] (Fig. 2A). The various LH units, which are bounded by the MCT on top and by the MBT at the base, consist of proterozoic sediments of Indian affinity that were accreted to the High Himalayan crystallines [e.g. [22,23]]. These units have a well developed foliation which depicts a broad antiform [9], interpreted as the result of a duplex [22,28] (Fig. 2A), that would have developed mainly over the last 10 Myr [22,23]. The structural architecture of the range suggests that the Himalayan wedge in Nepal has grown as a result of both frontal accretion due to successive activation of major thrust faults at front of the wedge and underplating due to the development of a duplex.

## 2.2. Kinematics

Holocene slip rate along the MFT, determined from geomorphic studies at the front of the range is  $21 \pm 1.5 \text{ mm yr}^{-1}$  [2]. Determinations of present day convergence from GPS studies range from 12 to 20 mm/yr [3,4,29,30]. The spread in GPS estimates may be explained by short term variations in time (within the seismic cycle) [31] and variations along strike related to extension in southern Tibet [29,32]. Processing of 8 years of continuous GPS and DORIS monitoring in Nepal suggests  $\sim 18 \text{ mm/yr}$  convergence for the modelled section [33]. We infer that convergence across the range is essentially the result of localized deformation along the MFT-MHT, internal shortening within the range being small.

Relatively young cooling ages suggest that the MCT may have been reactivated as an out of sequence thrust in the Pliocene [6,24,34] and may even still be active. The steep topographic front of the high range and the pattern of erosion across the Nepal Himalaya have been taken to suggest active thrusting of the MCT (e.g. [7]). Fluvial incision along the major Himalayan rivers in central Nepal increases abruptly from 1–2 mm/yr across the Lesser Himalaya to about 5 mm/yr across the Higher Himalaya where most rivers entrench into steep and narrow valleys with pronounced knickpoints [35]. This pattern definitely requires a zone with higher uplift rates along the front of the high range to prevent rivers from rapid headward erosion and maintain the smooth arcuate shape of the high range in map view. Active thrusting along the front of the high range, as argued for example by Wobus et al. [2003] [36] and Hodges et al. [2004] [7] might be a possibility. However, this would imply internal shortening of the Himalayan wedge at rates on the order of  $5\text{--}10 \text{ mm yr}^{-1}$  given the dip angle of the MCT, generally less than  $30^\circ$ . This in turn would imply

an implausible shortening rate across the range, in excess of  $26 \text{ mm yr}^{-1}$ . A possible alternative explanation for the pattern of erosion and topography across the range and for the young cooling ages at front of the High Range is a locally steeper dip angle along the basal thrust fault [35]. Here, we will hold the view that deformation has always been localized along a single major thrust fault, equivalent at present to the MHT, but that rocks can be

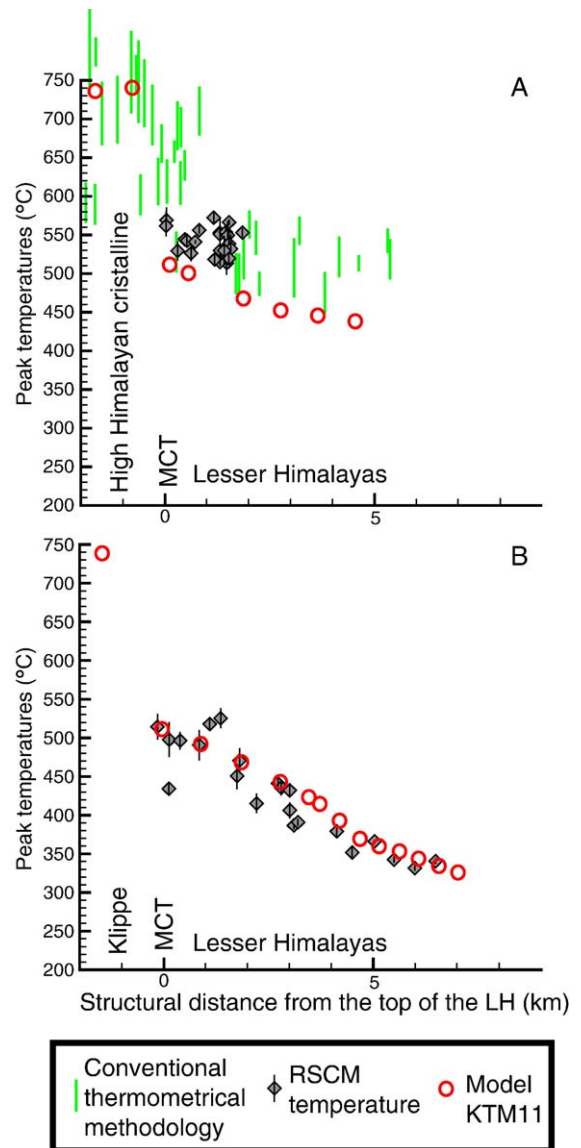


Fig. 3. Peak temperatures estimated from RSCM thermometry and conventional thermometry at, respectively, 80 km (A) and 50 km (B) from the front of the range in central Western Nepal. This compiled data set and the structural framework is presented and discussed in [27]. These data suggest an inverse thermal gradient which encompasses the topmost 7–8 km of Lesser Himalayan units. Circles show the prediction of model KTM11.

transferred from the footwall to the hanging wall as a result of forelandward migration of the thrust fault. In reality, the accretion process has probably been discrete with successive accretion of a limited numbers of LH thrust sheets [22,23]. Unfortunately, the structure of the LH does not allow for tightly constraining a discrete model. We will therefore assume that accretion has been a continuous process. In a reference frame defined by the MHT-MFT, the hanging wall is moving at an overthrusting velocity  $V_2$ , taken positive to the south, and the footwall is moving at an underthrusting velocity  $V_1$ , taken positive to the north. Fig. 2B shows the resulting trajectories. If the topography is assumed to be stationary and controlled by the geometry of the MHT and the implied pattern of uplift, sediment progradation onto the underthrusting Indian plate should be equal to  $V_1$ , a value estimated to be between 15 and 20 mm yr<sup>-1</sup> over the last 15 Myr [37]. In the following, we will assume that the underthrusting rate has not changed with time and take a value in this range. Provided that the thermal structure is determined, this kinematic model may then be used to predict the metamorphic grade and cooling ages of rocks collected at the surface.

### 3. Petrologic and radiometric constraints

#### 3.1. Petrologic constraints

The distribution of peak metamorphic temperatures in the Lesser Himalaya of Central Nepal has been recently documented from Raman Spectroscopy of Carbonaceous Material (RSCM) thermometry [26,27]. Peak metamorphic temperatures in the LH vary typically between 550°C near the MCT to about

350°C at deeper structural levels (Fig. 3A and B). The combination of these data with local structural measurements indicates that the peak metamorphic temperatures decrease downward in the section. This apparently inverted gradient was first documented near the MCT zone and is observed to actually encompass the topmost 5–7 km thick Lesser Himalayan units [27]. About 50 km north of the MBT these data show that the peak temperatures decrease by about 30°C/km on average with a break in slope about 4–5 km from the MCT. Closer to the MCT, the thermometric data show primarily a 150°C discontinuity at the MCT.

#### 3.2. Thermochronological constraints

The most complete picture of the chronology of cooling in central Nepal comes from <sup>39</sup>Ar/<sup>40</sup>Ar ages on muscovites (Fig. 4). This technique provides an estimate of the age of cooling of the rock sample through the muscovite bulk closure temperature assumed here to be ~350°C. These data indicate that the southern tip of the Kathmandu thrust sheet cooled below 350°C about 20–22 Myr ago, an age consistent with the onset of deformation and anatexis in the MCT zone [5,38]. The ages from the Kathmandu klippe and LH decrease gradually northwards to about 5 Myr at the front of the high range, following a nearly linear trend corresponding to a slope of about 0.24 Myr/km (Fig. 4). If internal deformation of the Himalayan crustal wedge has been minimal since about 20 Myr, this age gradient may be related to the overthrusting velocity, defined as the velocity of a nearly rigid wedge with respect to the thrust front [27]. It is important to note that the few muscovites collected from structural levels deeper than 6 km from

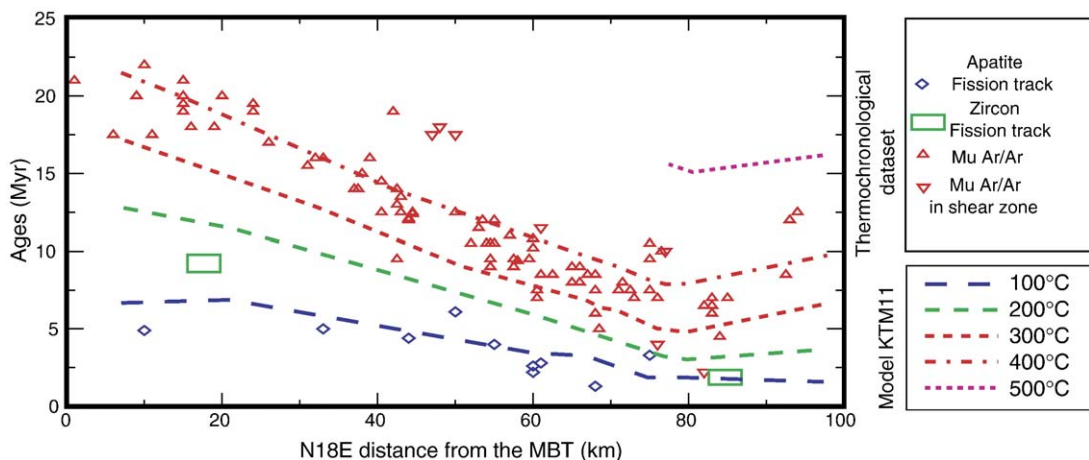


Fig. 4. Synthesis of thermochronological ages from the Lesser Himalaya and HHC across the Himalaya of Central Nepal (sources detailed in Fig. 1 caption). All data are reported along a N18E section together with the predicted cooling ages from model KTM11. See Fig. 1B for location of section.

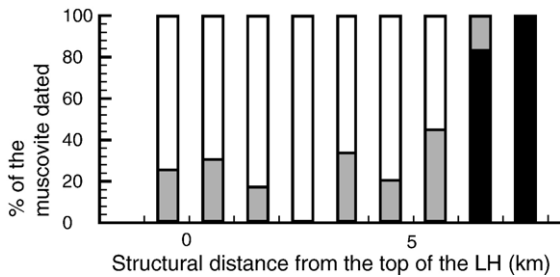


Fig. 5. Distribution of  $^{39}\text{Ar}/^{40}\text{Ar}$  ages obtained from muscovites as a function of structural distance from MCT. Reset (white), partially reset (grey) and non-reset (black) muscovites during the Himalayan orogenesis plot as a function of the structural distance from the top of the Lesser Himalayas. Samples collected at distance less than 5 km where dominantly reset. All non-reset samples were collected at more than 6 km structural distance from the MCT.

the top of the LH (Fig. 5) were apparently not reset for Ar [24,36,39]. This suggests that rocks below that structural level never crossed the  $350^\circ\text{C}$  isotherm, and puts additional constraints on the thermal structure. Sparser cooling ages from apatite and zircon fission tracks also depict ages decreasing northwards from the MBT to the front of the Himalayan range. Unfortunately, we do not have the information regarding the elevation of most of the samples so that we will assume that they were all collected along a simplified topographic surface.

#### 4. Model construction

##### 4.1. Geometry and kinematics

The model geometry is based on the concept of a single thrust zone (MHT) along which the Indian plate is subducted beneath the Himalayan front (Figs. 1 and 6).

The modeled domain is divided into 5 layers of uniform physical properties. These layers divide the footwall of the MHT into a mantle domain, the Indian lower crust taken to be 25 km thick, and a 15 km thick Indian Upper Crust (left side of the model). The hangingwall of the system is composed of the High Himalayan Crystalline and a Tethyan domain, with simple North dipping geometry (Fig. 6). The MHT is modelled as a 1 km thick shear zone with a constant dip angle ( $\alpha=10^\circ\text{N}$ ) and the model origin is taken at the intersection of the MHT plane with the topographic surface. Accretion is modelled by allowing continuous material transfer through the shear zone in the underplating window (Fig. 6). The topography, culminating at 5 km in Southern Tibet, is assumed to be steady-state, meaning that erosion compensates exactly the uplift rate everywhere. Erosion thus comprises one uniform term related to the sliding of the Himalayan wedge on the MHT, and a spatially varying term related to the material accretion flux through the MHT.

The velocity field is constructed in order to satisfy the continuity equation ( $\nabla \cdot \vec{v} = 0$ ), which implies continuity of the fault-normal velocity, deformation within the sliding blocks is approximated by vertical shear. The horizontal velocity component is thus uniform within the footwall and hanging wall of the MHT. Horizontal velocities of footwall and hanging wall in the model reference frame are, respectively,  $V_1$  and  $-V_2$ . The sum  $V_1 + V_2$ , which represents the convergence rate across the range, was chosen to match the 21 mm/yr ( $\pm 1.5$ ) Holocene shortening rate [2]. Then, the vertical components of the velocity are  $(tg\alpha \cdot V_2 + V_u(x))$  for the hanging wall and  $(-tg\alpha \cdot V_1 + V_u(x))$  for the footwall, where  $V_u(x)$  represents the underplating (accretion) velocity at position  $x$ . The fault normal velocity is thus  $\cos\alpha \cdot V_u$  and the continuity equation is satisfied. For an

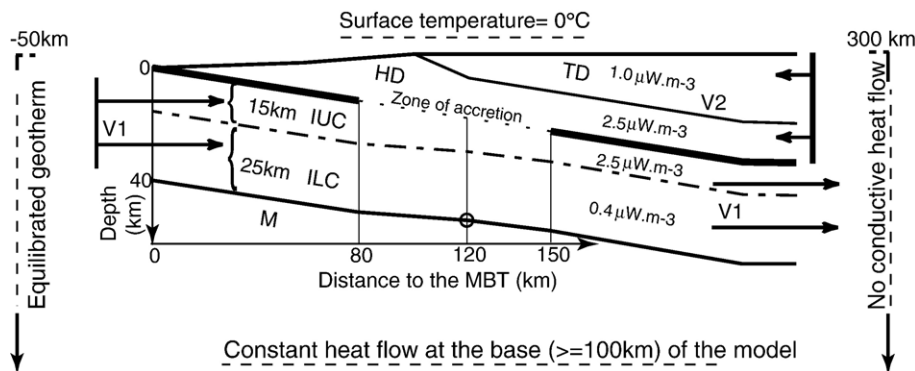


Fig. 6. Model geometry, kinematic and thermal parameters used in model KTM11 (cf. Tables 1–3 for additional parameters).

Table 1  
Physical parameters for crust and mantle

|   |                        |                      |
|---|------------------------|----------------------|
| Heat capacity ( $\text{Jm}^{-3}$ )  | $\rho_c$               | $2.5 \times 10^6$    |
| Mantle density at $0^\circ\text{C}$ $10^5\text{Pa}$ ( $\text{kgm}^{-3}$ ) | $\rho_{\text{mantle}}$ | 3350                 |
| Thermal diffusivity ( $\text{m}^2\text{s}^{-1}$ )                         | $\kappa$               | $10^{-6}$            |
| Thermal expansion coefficient ( $\text{K}^{-1}$ )                         | $\chi$                 | $2.4 \times 10^{-5}$ |

accretion window of width  $L$  (measured along the  $x$  axis), the velocity of underplating is related to the thickness  $\Delta z$  of material scraped from the top of the Indian crust by the equation:

$$V_u = V_1 \Delta z / L.$$

Considering that the formation of the Lesser Himalayan duplex occurred over the last 8–10 Ma [22,23] whereas the accretion of Lesser Himalayan slivers into the MCT zone spanned a longer time scale (up to about 20 Ma), we define two kinematic phases.

During the first phase an underplating velocity of 0.3 to 0.5 mm/yr is applied between 80 and 150 km to account for the ductile growth of the MCT zone. During the second phase, the underplating velocity is increased to 1–1.5 mm/yr in the 80–120 km interval to account for the accretion of the duplex units. These underplating velocities have a strong influence on the modeling results, as well as on the predicted geometry of the Himalayan wedge, and the best combination of parameters will be discussed in Section 5.3.

#### 4.2. Thermal modeling

The heat transport problem is treated in the steady and transient states with the FEAP finite element program, using a Galerkin formulation in a Eulerian frame [40]. The first kinematic phase (20–8 Ma) is treated as a thermal steady-state, and is taken as the initial conditions for the second kinematic phase, which is solved in transient state. Computation of peak  $T$  and

cooling ages are then performed by particle tracking through the time-dependent temperature field. The equation solved includes diffusion, advection, and heat production source terms:

$$\rho c_p \left( \frac{\partial T}{\partial t} + \vec{v} \cdot \vec{\nabla} T \right) = \nabla k \nabla T + A_R + A_S \quad (1)$$

where  $\rho$  is density,  $c_p$  is the specific heat,  $\vec{v}$  is velocity,  $T$  is temperature,  $t$  is time,  $k$  is the thermal conductivity while  $A_R$  and  $A_S$  are, respectively, the radiogenic heat production and the shear heating. While  $A_R$  is deduced from the petrochemical composition of the various domains defined in the model,  $A_S$  is computed in prescribed shear zones from the velocity discontinuity  $\Delta v$ , the thickness of the shear zone  $e$  and the shear stress  $\tau$  with  $A_S = \frac{\tau \times \Delta v}{2e}$ . In the brittle domain, the shear stress is computed as a function of the lithostatic pressure  $P_1$  and a friction coefficient  $\chi$  with:

$$\tau = 2\chi \times P_1 \quad (2)$$

In the ductile domain, the shear stress is deduced from a power flow law:

$$\tau^n = \frac{\dot{\epsilon}}{A \times e^{\frac{Q}{RT}}} \quad (3)$$

where  $\dot{\epsilon}$  is the strain rate,  $A$  and  $n$  are intrinsic medium parameters,  $Q$  is an activation energy,  $R$  is the universal gas constant. A maximum value for shear stress may also be applied in both domains.

#### 4.3. Model parameters

Model parameters may primarily influence the temperature field or the velocity field. Thermal parameters influence only the temperature field. These are heat conductivity, heat capacity (and heat diffusivity, which is a combination of both parameters), radioactive

Table 2  
Specific physical parameters for each layer in KTM11 model

| Layer | Thermal conductivity ( $\text{W m}^{-1} \text{K}^{-1}$ ) | Radiogenic heat production ( $\mu\text{W/m}^3$ ) | Chemical composition | Compressibility ( $\text{Pa}^{-1}$ ) | Layer thickness (km)                  |
|-------|--|--|----------------------|--------------------------------------|---------------------------------------|
| TD    | 2.5  | 1.0  | Granodioritic        | $2 \times 10^{-11}$                  | Variable (Fig. 6)                     |
| HD    | 2.5  | 2.5  | Granodioritic        | $2 \times 10^{-11}$                  | Variable (Fig. 6)                     |
| IUC   | 2.5  | 2.5  | Granodioritic        | $2 \times 10^{-11}$                  | 15 km on the Indian side of the model |
| ILC   | 2.5  | 0.4  | Intermediate         | $1 \times 10^{-11}$                  | 25 km                                 |
| M     | 3.0  | 0.0  | Peridotitic          | $8 \times 10^{-12}$                  | Variable                              |

Abbreviations: M, mantle; ILC, Indian lower crust; IUC, Indian upper crust; HD, Himalayan domain; TD, Tethyan domain.

Table 3  
Parameters used for the shear heating computation in KTM11

| $\tau_{\max}$<br>(MPa) | Brittle mode |        | Ductile mode                    |     |                 |
|------------------------|--------------|--------|---------------------------------|-----|-----------------|
|                        | $e$<br>(m)   | $\chi$ | Granite flow law                |     |                 |
|                        |              |        | $A$<br>(MPa $^{-n}$ s $^{-1}$ ) | $n$ | $Q$<br>(kJ/mol) |
| 50                     | 1000         | 0.1    | $2.512 \times 10^{-9}$          | 3.4 | 139             |

Shear stresses do not exceed 50MPa, a value consistent with maximum deviatoric stresses obtained by comparing seismicity and current geodetic strain [32]. Granite flow law from [55].

heat production, thermal boundary conditions and the rheological parameters controlling the shear heating on the MHT. Parameters influencing the velocity field (kinematic parameters) also influence the temperature field through the advection term in Eq. (1). The budget of accretion and erosion notably affects the thermal regime [11,13]. Once the geometry of the MHT is set, the velocity field in our kinematic description depends on the underthrusting ( $V_1$ ) and overthrusting ( $V_2$ ) velocities and on the spatial and temporal distribution of material flux through the MHT (see Section 4.1).

The temperature field thus depends on a large number of parameters. Multiple trade offs occur, between thermal parameters such as basal heat flow, radiogenic heat generation and shear heating, and also between thermal parameters and kinematic parameters. Geophysical and petrological constraints thus define a possible range of physical parameters (rather than a unique set of parameters), which can account for the steady-state thermal regime in the Himalayas [11–13]. Based on these modeling studies, we define a starting model (KTM1) and discuss how variations in parameters affect results based on a series of model runs (Table 4). Our final (and preferred) model, KTM 11, uses the same thermal parameters as KTM 1 but with kinematic parameters tuned for better adjustment to Upper Indian Crust (UIC) geometry and total accreted volume. Both models yield similar results in terms of peak temperatures and thermochronological evolution.

In all models, the left and right hand side boundary conditions are, respectively, fixed temperature conditions corresponding to a relaxed steady-state geotherm along the Indian side and no lateral heat flow along the Tibetan side. The upper and lower boundary conditions are  $0^\circ\text{C}$  and a constant basal heat flow ( $15\text{mW/m}^2$ ), representative of the Indian cratons [41]. Thermal diffusivity is taken uniform at  $10^{-6}\text{m}^2/\text{s}$ , mantle thermal conductivity is set to  $3\text{Wm}^{-1}\text{K}^{-1}$  and crust thermal conductivity is set to  $2.5\text{Wm}^{-1}\text{K}^{-1}$  [12] (Table 2). In KTM 1 and 11, the radiogenic heat

production of the UIC and HHC is taken to be homogeneous and equal to  $2.5\text{mW/m}^3$ , which agrees with previously determined HHC heat productions [42]. A lower crustal radiogenic heat production of  $0.4\text{mW/m}^3$  is used [43]. Metamorphic facies and rock densities are determined from petrogenetic grids [44]. Rock densities are then integrated with depth to calculate the lithostatic pressure, which is needed to calculate the shear heating on the MHT. The shear heating calculation is the only step in which

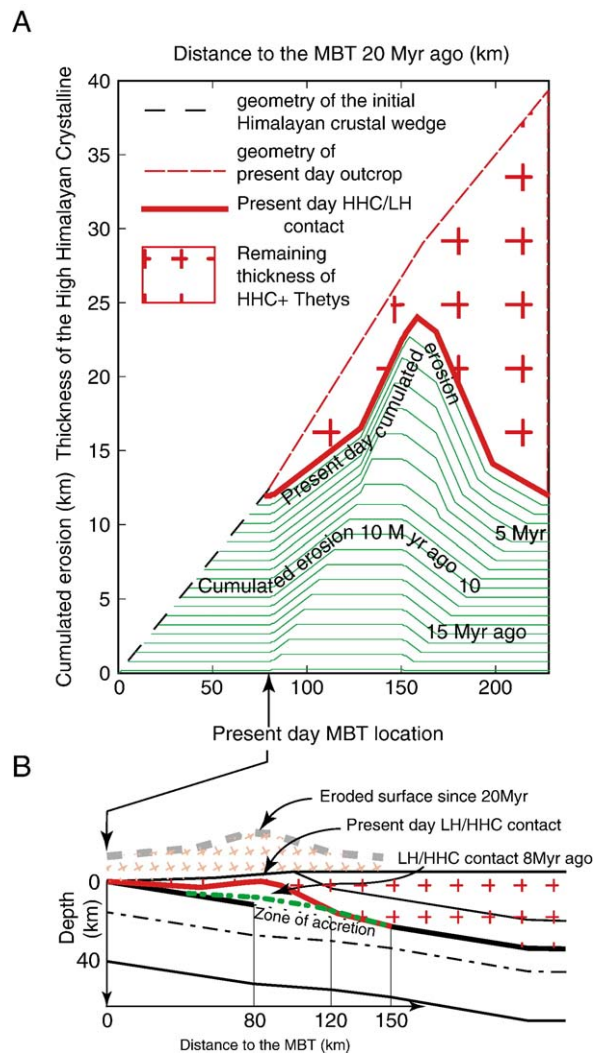


Fig. 7. A—Cumulated erosion through time (0–20Ma) from model KTM11 illustrating underplating and erosion focus at the front of the present day high Himalayan range due to the slow overthrusting velocity. The present day HHC and Tethyan Himalayan thicknesses (red crosses) as well as the total amount of material accreted (green) are materialized. B—Geometry of the LH/HHC contact in KTM11 model at present day (red line) and 8Myr ago (green dashed line). The surface eroded since 20Myr is materialized by the thick grey dashed line.



mechanics are involved in the model. In KTM 1 and 11, shear heating is computed with the same moderate friction law as used by Henry et al. [1997] [12]. A flow law for granite is used in the ductile domain, and a 50MPa value is assumed for the maximum shear stress in both brittle and ductile domains (Table 3). The transition from brittle to ductile rheologies in the shear zone occurs at a temperature of about 400°C, corresponding to about 18km depth on the Main Himalayan Thrust.

## 5. Forward modeling results and comparison with data

### 5.1. Overthrusting velocity and thermochronological data

Model KTM11 predicts a cooling history consistent with the various thermochronological data, which are relatively well distributed both in time (the data spans the last 20Myr) and in space along the section (Fig. 4). This model yields a uniform age gradient between the Main Boundary Thrust and 80km, for closing temperatures of 350 and 400°C. This result is tied to the assumption of a zone of increased erosion at the front of the high range. Models with uniform erosion over the Himalayan wedge [e.g. [12]] fail to

reproduce this gradient. The zone of increased erosion may be reproduced by assuming a crustal ramp or, as in this study, by underplating. The value of the age gradient is given to be the inverse of the overthrusting rate [27] (model parameter  $V_2$ ). The observed 0.24Ma/km suggest an overthrusting rate of about 4mm/yr. The trend in Ar–Ar cooling ages is indeed well adjusted for  $V_2=4\pm 0.5$ mm/yr and  $V_1=17\pm 0.5$ mm/yr (Fig. 4).

The uncertainty on the 0.24Ma/km Ar/Ar muscovite age gradient along the Kathmandu transect follows from the 5Ma scattering around the average linear trend (Fig. 4). Considering that this gradient is well defined over a 60km width, the corresponding uncertainty on the gradient is  $\pm 0.04$ Ma/km, and the range of compatible overthrusting velocities  $V_2$  is 3.5–5.0mm/yr.

The model yields minimum  $^{39}\text{Ar}/^{40}\text{Ar}$  ages on muscovite of the order of 7Ma and zircon and apatite fission track ages, respectively, around 4 and 2Ma (Fig. 4). For apatite, the minimum ages are obtained over the zone of maximum erosion and increase sharply to a nearly constant value south of it. While this feature is reproduced in the model, the predicted fission track ages (assuming closure temperature at 120°C for apatite and 230°C for zircon) appears to be younger. This could be explained if the increase of

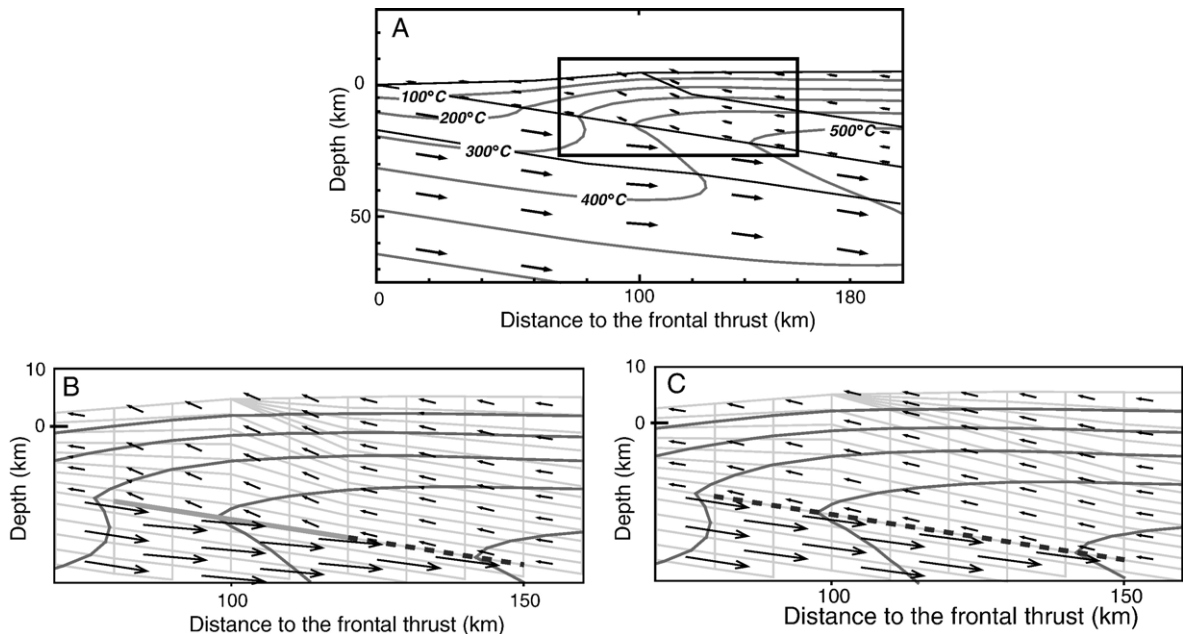


Fig. 8. A—Present thermal structure and velocity field computed from model KTM11. Arrows show velocity with respect to MHT corresponding to the kinematics over the last 8 Myr. Box shows location of close up views in B and C. B—Close up view corresponding to the box in A. C—Velocity field computed from model KTM11 for the 20–12Ma period and thermal structure at 8Ma.

erosion rates since 8Ma affected a wider zone than just the underplating window. However, additional dense and well geo-referenced low temperature thermochronometrical data are required before being able to constrain this assumption considering the numerous sources of uncertainties (altitude, compositional and diffusion size parameters, the model predicting also highly variable 15 to 100 °C/Ma cooling rates through the 90–230 °C isotherms inducing variations of bulk closure temperature for thermochronometers in that range).

### 5.2. Parameters of underplating and peak temperature

The position of the accretion window and the rate of underplating determine the gradient of peak metamorphic temperatures as well as the geometry of the underplated body and distribution of erosion at the surface (Fig. 7A and B). In the Lesser Himalayan domain of the model, the peak temperature is reached at the time of underplating, or shortly afterwards. Peak metamorphic temperatures in the 300–550 °C range of observed values in the LH constrain the position of the zone of underplating. With the thermal parameters in models KTM1 and 11, the extent of the underplating window must lie from about 80 to about 150 km from the MBT.

We assume that from 20 to 8Ma the top 1.4 km of the Indian crust is underplated through a 70 km wide window (80 to 150 km from MFT (Figs. 6–8)). The corresponding accreted flux is  $24 \text{ km}^3 \text{ Ma}^{-1} \text{ km}^{-1}$ . Between 8 Ma and present, an additional flux of  $30 \text{ km}^3 \text{ Ma}^{-1} \text{ km}^{-1}$  is applied between 80 and 120 km from the MBT, by increasing the accretion rate to  $1.5 \text{ mm yr}^{-1}$  through that window. The flux of underplated material is then  $55 \text{ km}^3 \text{ Ma}^{-1} \text{ km}^{-1}$ , corresponding to the top 3.2 km of the Indian crust. The uplift rate is about  $1.5 \text{ mm yr}^{-1}$  over the zone with maximum underplating rate (80–120 km). The predicted present day geometry involves a frontal synform with preserved HHC and a large anticlinorium at the front of the range (Fig. 7B). The total amount of material accreted is  $720 \text{ km}^3 \text{ km}^{-1}$  (Fig. 7A). This geometry is consistent with the simplified structural section across the Kathmandu Klippe (e.g. Fig. 2A) where the accreted LH volume can be estimated to between 500 and  $1000 \text{ km}^3 \text{ km}^{-1}$ .

The range of temperatures along the midcrustal zone of accretion matches with the peak temperatures deduced from RSCM thermometry (Figs. 3 and 8). The predicted peak temperatures match the inverse apparent gradient estimated 50 km from the MBT (Fig. 9). The break-in-slope at about 5 km structural distance from the MCT might reflect the change in rate of

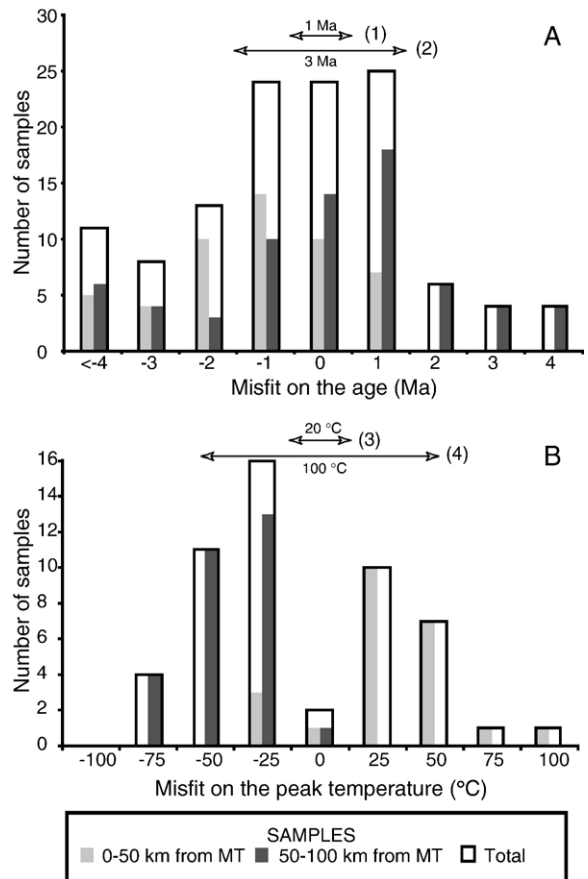


Fig. 9. Misfits on the peak temperatures and the ages at which the samples have gone through the 350 °C isotherm, assuming a muscovite bulk closure temperature at 350 °C, a reasonable value for the 30 to 50 °C/Ma cooling rates generated in the model [54]. It appears that, while the misfits distributions are centred, the southernmost dataset (sampled within 0–50 km from the MBT) is cooler and older than predicted whereas the northernmost one is hotter and younger. This trend probably reflects complexities not accounted for in the model such as a decrease of the total velocity on the MHT since 20 Ma and/or an increase of erosion rates in the high range, possibly related to out-of-sequence thrusting along the MCT zone.

accretion around 8 Myr. The model also reproduces well the peak metamorphic temperatures across the MCT (Fig. 3A and B). It should be noted that the model predicts peak temperatures lower than 350 °C in the core of the anticlinorium at structural distances as short as 5 km from the top of the LH, consistent with the presence of non-reset muscovites (Fig. 5). The model therefore can explain altogether the relationship between the structural location of the reset and no-reset transition zone and the location at the front of the High Himalayan Range of the rapidly eroded domain as well as the cooling history of the klippen at the front of the system.

Table 4  
Thermal and kinematic parameters used in models discussed

| Model   | Radiogenic heat production ( $\mu\text{W}/\text{m}^3$ ) | Boundary velocities ( $\text{mm yr}^{-1}$ ) |            | Vuz(x) ( $\text{mm an}^{-1}$ ) |                             | Final LH volume ( $\text{km}^3 \text{ km}^{-1}$ ) | Shear heating model |
|---------|---|---|------------|--------------------------------|-----------------------------|---|---------------------|
|         | IUC and HHC   | $V_1$                                       | $V_2$      | 80 < x < 120 km<br>20–8/8–0 Ma | 120 < x < 150 km<br>20–0 Ma |   | Ductile rheology    |
| KTM1    | 2.5   | 20  | 4.2        | 0.44/1.32                      | 0.44                        | 893   | Granite             |
| KTM7VM  | 2.5   | <u>18</u>                                   | 4.2        | <b>0.40/1.20</b>               | <b>0.40</b>                 | <b>805</b>  | Granite             |
| KTM7VP  | 2.5   | <u>21</u>                                   | 4.2        | <b>0.48/1.45</b>               | <b>0.48</b>                 | <b>981</b>  | Granite             |
| KTM7R1  | 1.5   | 20  | 4.2        | 0.44/1.32                      | 0.44                        | 893   | Granite             |
| KTM7R2  | <u>2.0</u>  | 20  | 4.2        | 0.44/1.32                      | 0.44                        | 893   | Granite             |
| KTM7SZ2 | 2.5   | 20  | 4.2        | 0.44/1.32                      | 0.44                        | 893   | <u>Diabase</u>      |
| KTM11   | 2.5   | 21  | <u>4.0</u> | <u>0.34/1.09</u>               | <u>0.34</u>                 | <b>723</b>  | Granite             |

Varied parameters are underlined.  $V_2$  and  $V_1$  are, respectively, the overthrusting velocity and total velocity on the MHT.  $V_1$ , the underthrusting velocity is thus  $V_1 - V_2$ . Note that changes in  $V_1$  induce changes in Lesser Himalayas evolution in the model (bold italic).

### 5.3. Parameter sensitivity and trade offs

We have run a number of models (listed in Table 4) to assess the sensitivity of the model to the parameters and possible trade-offs. As discussed above,  $V_2$  controls the gradient of exhumation ages along the section which were quite tightly constrained from the available data. We therefore did not vary this parameter.

A decrease in  $V_1$ , (i.e. down to  $13.8 \text{ mm yr}^{-1}$  in model KTM7VM) induces a decrease in the volume of LH accreted ( $85 \text{ km}^3 \text{ km}^{-1}$ ) as well as a small increase in maximum peak temperature ( $\sim 10^\circ\text{C}$ ). This is because the temperature at any given point increases when the underthrusting velocity decreases. An increase in  $V_1$  (e.g. up to  $16.8 \text{ mm yr}^{-1}$  in KTM7VP) has the opposite effect. So varying  $V_1$  within a reasonable range of values ( $\pm 20\%$ ), in view of the constraints brought by the rate of sediment progradation over the foreland, has small effect on peak metamorphic temperatures and cooling ages but change significantly ( $\pm 20\%$ ) the time needed to accrete the volume of material corresponding to the Lesser Himalayan duplex.

The thermal structure is more sensitive to radioactive heat production variations tested in models KTM7R1 to 3. Decreasing radiogenic heat productions to 2.0 and  $1.5 \mu\text{W m}^{-3}$  decreases the LH peak temperature by about 30 and  $70^\circ\text{C}$ , respectively, if the location of the underplating window is not changed. The lower temperatures in the model could, however be compensated by a northward shift of the accretionary window (up to 30 or 50 km, respectively).

Shear heating has also a strong influence on the temperature field. In model KTM7SZ2, a diabase ductile rheology is used and the maximum shear stress

set at 100 MPa (instead of granite rheology and 50 MPa maximum shear stress). Peak temperatures for the accreted LH reach 430 to  $590^\circ\text{C}$ , about  $100^\circ\text{C}$  hotter than in the preferred model KTM11. If only the peak metamorphic temperature dataset is considered, this could be compensated by a 70 km southward shift of the underplating window.

These northward or southward shifts of the accretionary window in models KTM7SZ2 or KTM7R1 would result in a position of the Lesser Himalayan body relative to the thrust front which would be incompatible with the structural constraints. In theory the position of this body also depends on  $V_2$ , constrained largely independently from the gradient of  $^{39}\text{Ar}/^{40}\text{Ar}$  muscovite ages (cf. Section 5.1).

Hence the model we propose is certainly non-unique due to various trade-offs among model parameters. In particular, it is possible to compensate a change in the thermal structure by adjusting the geometry of the accretionary window so as to still be in good agreement with the peak metamorphic temperature (we need the accretionary window to span a range of temperatures going from about 550 down to about  $320^\circ\text{C}$ ).

Regarding the model prediction in terms of cooling ages, there is also a trade off between the gradient of temperature with depth and the uplift rate. For example, if the geotherms become steeper due to change in the thermal parameters (e.g. an increase of shear heating or of radiogenic heat production), the cooling ages might still be matched reasonably well by decreasing uplift rates (assumed equal to erosion rates). In the absence of good vertical transects of cooling ages in the Lesser Himalaya, however, this kind of trade-off cannot be resolved.

## 6. Discussion and conclusion

We have presented numerical models that illustrate the effect of localized underplating and of temporal changes in the velocity field within a slowly varying thermal structure. Comparison of the modelling results with thermochronologically constrained cooling age profiles suggest that the age minimum observed along the MCT trace may primarily be related to the distribution of underplating and erosion. The continuous trend in the muscovite age profile defines an age gradient we tie to the overthrusting velocity. The age gradient and the inferred kinematic model also suggests that the earliest thermal history of the system should be depicted at the fore-edge of the hangingwall of the Himalayan orogen.

This model ignores the role of the South Tibetan Detachment which has likely been active in the early period covered by our model. Coeval thrust motion along the MCT and normal motion along the STD between 16 and 20Ma [45,46] would have allowed rapid exhumation of the HHC, possibly as a result of midcrustal channel flow [e.g. [20,47,48]]. But this effect is not considered here as most of the data we analyze pertains to the more recent tectonic history of the range.

The dataset used here has been generated projecting thermometrical as well as thermochronological data acquired along strike in a region encompassing lateral variations. The model, thus, might be considered as appropriate only on average for the Kathmandu area where a HHC klippe has been preserved. It probably corresponds to a low underplating/ low erosion end member. Modelling the LH geometry on transects on either side of the Kathmandu klippe would require a longer phase of duplex formation and/or higher underplating rates. Furthermore, the projection of the thermochronological data acquired along strike, in whatever geological unit, structural distances to the main shear zone or altitudes, might contribute significantly to the scattering of  $^{39}\text{Ar}/^{40}\text{Ar}$  cooling ages. This loose distribution does not allow for refining the hangingwall velocity value or even constrain the continuity/discontinuity of the underplating mechanisms. Finally, the topographical effects, critical to the interpretation of FT data [49] in settings with high local relief (i.e.  $\sim 2\text{km}$  in our region of interest), ought to be taken into account. Indeed, the high erosion rates generated by the model, in the range  $0.7\text{--}2.2\text{kmMa}^{-1}$ , should induce a 1–3Ma scattering in  $^{39}\text{Ar}/^{40}\text{Ar}$  age well correlated to the topography.

In spite of its non-uniqueness, the forward model presented here reconciles the kinematic of mountain

building in the Himalayas that can be inferred from structural geology, morphotectonic studies, and available thermo-metamorphic and thermo-chronological data implying that the Himalayan wedge would have grown essentially as a result of underplating during the last 8Myr. Given the range of temperature at the depths of interest this process likely occurs in the transition zone between the brittle (seismogenic) and ductile portions of the MHT. The similar kinematics inferred from exhumed thrust fault systems [50] suggests that this process might be a common mode of crustal thickening. The data requires a major increase of the accretionary flux about 8Myr ago corresponding to the development of the LH midcrustal duplex. The model presented here is based on critical assumptions: the topography is assumed steady-state and underplating is modelled as a continuous process. Nonetheless, we believe it provides a first order kinematic description of the Nepal Himalayas evolution over the last 10–20Ma, tying together a variety of structural, geochronological and petrological data. Furthermore, it indicates that short term kinematics, determined at the seismic cycle and Holocene time-scales, are consistent with the long term evolution of the High Himalayan range, over at least 10 million years. The model does not account for late MCT reactivation, nor disproves it, but suggests this process may not be essential to explain first order observations of structure and metamorphism on the Kathmandu transect.

## Acknowledgements

The authors are thankful to Patrick Lefort, Maurice Brunel and Arnaud Pêcher for sharing with them their experience of Himalayan tectonics. This study has also benefited from discussion with Peter Copeland who kindly authorized us to use his collection of Ar/Ar ages. Finite-element computations were done with the FEAP program, developed by R. Taylor at the University of California at Berkeley. We are most grateful to T. Ehlers, P. Tapponnier, K. Whipple and anonymous reviewers for their comments and suggestions which greatly helped in improving the manuscripts. This is Caltech Tectonics Observatory contribution no 34.

## References

- [1] Y. Makovsky, S.L. Klempner, H. Liyan, L. Deyuan, P.I. Team, Structural elements of the southern Tethyan Himalaya crust from wide-angle seismic data, *Tectonics* 15 (1996) 997–1005.
- [2] J. Lavé, J.-P. Avouac, Active folding of fluvial terraces across the Siwaliks Hills, Himalayas of central Nepal, *J. Geophys. Res.* 105 (2000) 5735–5770.

- [3] R. Bilham, K. Larson, J. Freymueller, P.I. members, GPS measurements of present-day convergence across the Nepal Himalaya, *Nature* 386 (1997) 61–64.
- [4] K. Larson, R. Bürgmann, R. Bilham, J.T. Freymueller, Kinematics of the India–Eurasia collision zone from GPS measurements, *J. Geophys. Res.* 104 (1999) 1077–1093.
- [5] M.S. Hubbard, T.M. Harrison,  $^{40}\text{Ar}/^{39}\text{Ar}$  age constraints on deformation and metamorphism in the Main Central Thrust zone and Tibetan slab, Eastern Nepal Himalaya, *Tectonics* 8 (1989) 865–880.
- [6] T.M. Harrison, F.J. Ryerson, P. Le Fort, A. Yin, O.M. Lovera, E.J. Catlos, A late Miocene–Pliocene origin for the central Himalayan inverted metamorphism, *Earth Planet. Sci. Lett.* 146 (1997) E1–E8.
- [7] K.V. Hodges, C. Wobus, K. Ruhl, T. Schildgen, K. Whipple, Quaternary deformation, river steepening, and heavy precipitation at the front of the Higher Himalayan ranges, *Earth Planet. Sci. Lett.* 220 (2004) 379–389.
- [8] T.A. Ehlers, Crustal thermal processes and the interpretation of thermochronometer data, *Rev. Mineral. Geochem.* 58 (2005) 315–350.
- [9] A. Pêcher, The metamorphism in Central Himalaya, *J. Metamorph. Geol.* 7 (1989) 31–41.
- [10] M.L. Hauck, K.D. Nelson, L.D. Brown, W. Zhao, A.R. Ross, Crustal structure of the Himalayan orogen at 90deg east longitude from project INDEPTH deep reflection profiles, *Tectonics* 17 (1998) 481–500.
- [11] L.H. Royden, The steady state thermal structure of eroding orogenic belts and accretionary prisms, *J. Geophys. Res.* 98 (1993) 4487–4507.
- [12] P. Henry, X. Le Pichon, B. Goffé, Kinematic, thermal and petrological model of the Himalayas: constraints related to metamorphism within the underthrust Indian crust and topographic elevation, *Tectonophysics* 273 (1997) 31–56.
- [13] A.D. Huerta, L.H. Royden, K.V. Hodges, The effects of accretion, erosion and radiogenic heat on the metamorphic evolution of collisional orogens, *J. Metamorph. Geol.* 17 (1999) 349–366.
- [14] P. Le Fort, Himalaya : the collided range: present knowledge of the continental arc, *Am. J. Sci.* 275A (1975) 1–44.
- [15] P. Bird, Initiation of intracontinental subduction in the Himalaya, *J. Geophys. Res.* 83 (1978) 4975–4987.
- [16] P. Molnar, P. England, Temperatures, heat flux and frictional stress near major thrust faults, *J. Geophys. Res.* 95 (B4) (1990) 4833–4856.
- [17] M. Brunel, J. Andrieux, Sur un modèle explicatif du métamorphisme inverse himalayen, *Cr. Acad. Sci. D* 291 (1980) 609–612.
- [18] M.S. Hubbard, Ductile shear as a cause of inverted metamorphism: example from the Nepal Himalaya, *J. Geol.* 104 (1996) 493–499.
- [19] M.P. Searle, A.J. Rex, Thermal model for the Zaskar Himalaya, *J. Metamorph. Geol.* 7 (1989) 127–134.
- [20] D. Grujic, M. Casey, C. Davidson, L.S. Hollister, R. Kündig, T. Pavlis, S. Schmid, Ductile extrusion of the Higher Himalayan crystalline in Bhutan: evidence from quartz microfabrics, *Tectonophysics* 260 (1996) 21–43.
- [21] C. Beaumont, R.A. Jamieson, M.H. Nguyen, B. Lee, Himalayan tectonics explained by extrusion of a low-viscosity crustal channel coupled to focused surface denudation, *Nature* 414 (2001) 738–742.
- [22] P.G. DeCelles, D.M. Robinson, J. Quade, T.P. Ojha, C.N. Garzzone, P. Copeland, B.N. Upreti, Stratigraphy, structure, and tectonic evolution of the Himalayan fold-thrust belt in western Nepal, *Tectonics* 20 (2001) 487–509.
- [23] D.M. Robinson, P.G. DeCelles, P.J. Patchett, C.N. Garzzone, The kinematic evolution of the Nepalese Himalaya interpreted from Nd isotope, *Earth Planet. Sci. Lett.* 192 (2001) 507–521.
- [24] E.J. Catlos, T.M. Harrison, M.J. Kohn, M. Grove, F.J. Ryerson, C. E. Manning, B.N. Upreti, Geochronologic and thermobarometric constraints on the evolution of the Main Central Thrust, central Nepal Himalaya, *J. Geophys. Res.* 106 (2001) 16177–16204.
- [25] M.J. Kohn, E.J. Catlos, F.J. Ryerson, T.M. Harrison, Pressure–temperature–time path discontinuity in the Main Central Thrust zone, central Nepal, *Geology* 29 (7) (2001) 571–574.
- [26] O. Beyssac, L. Bollinger, J.P. Avouac, B. Goffé, Thermal metamorphism in the Lesser Himalaya of Nepal determined from Raman spectroscopy of carbonaceous material, *Earth Planet. Sci. Lett.* 225 (2004) 233–241.
- [27] L. Bollinger, J.P. Avouac, O. Beyssac, E.J. Catlos, T.M. Harrison, M. Grove, B. Goffé, S. Sapkota, Thermal structure and exhumation history of the lesser Himalaya in central Nepal, *Tectonics* 23 (2004) TC5015, doi:10.1029/2003TC001564.
- [28] D. Schelling, K. Arita, Thrusts tectonics, crustal shortening and the structure of the Far Eastern Nepal Himalaya, *Tectonics* 10 (1991) 851–862.
- [29] Q.Z. Chen, J.T. Freymueller, Q. Wang, Z.Q. Yang, C.J. Xu, J.N. Liu, A deforming block model for the present-day tectonics of Tibet, *J. Geophys. Res.* 109 (B1) (2004) (art. no.-B01403).
- [30] F. Jouanne, J.L. Mugnier, J.F. Gamond, P. Le Fort, M.R. Pandey, L. Bollinger, M. Flouzat, J.P. Avouac, Current shortening across the Himalayas of Nepal, *Geophys. J. Int.* 157 (1) (2004) 1–14.
- [31] H. Perfettini, J.P. Avouac, Stress transfer and strain rate variations during the seismic cycle, *J. Geophys. Res.* 109 (B2) (2004) B02304.
- [32] L. Bollinger, J.P. Avouac, R. Cattin, M.R. Pandey, Stress buildup in the Himalaya, *J. Geophys. Res.* 109 (2004) B11405, doi:10.1029/2003JB002911.
- [33] P. Bettinelli, J.P. Avouac, M. Flouzat, F. Jouanne, L. Bollinger, P. Willis, G.R. Chitrakar, in press. Plate motion of India and interseismic strain in the Nepal Himalaya from GPS and DORIS measurements, *J. Geod.*
- [34] T.M. Harrison, M. Grove, O.M. Lovera, E.J. Catlos, A model for the origin of Himalayan anatexis and inverted metamorphism, *J. Geophys. Res.* 103 (1998) 27017–27032.
- [35] J. Lavé, J.P. Avouac, Fluvial incision and tectonic uplift across the Himalayas of Central Nepal, *J. Geophys. Res.* 106 (2001) 26561–26592.
- [36] C.W. Wobus, K.V. Hodges, K.X. Whipple, Has focused denudation sustained active thrusting at the Himalayan topographic front? *Geology* 31 (2003) 861–864.
- [37] J.P. Avouac, Mountain building, erosion, and the seismic cycle in the Nepal Himalaya, *Adv. Geophys.* 46 (2003) 1–80, doi:10.1016/S0065-2687(03)46001-9.
- [38] K.V. Hodges, R. Parrish, M.P. Searle, Tectonic evolution of the central Annapurna range, Nepalese Himalaya, *Tectonics* 15 (1996) 1264–1291.
- [39] P. Copeland, T.M. Harrison, K.V. Hodges, P. Marujeol, P. Le Fort, A. Pêcher, An early Pliocene thermal disturbance of the Main Central Thrust, central Nepal: implications for Himalayan tectonics, *J. Geophys. Res.* 96 (1991) 8475–8500.
- [40] O.C. Zienkiewicz, R.L. Taylor, *The Finite Element Method*, McGraw-Hill, New York, 1989.
- [41] M.L. Gupta, Is the Indian shield hotter than other Gondwana shields? *Earth Planet. Sci. Lett.* 115 (1993) 275–285.

- [42] P.C. England, P. Le Fort, P. Molnar, A. Pêcher, Heat sources for Tertiary metamorphism and anatexis in the Annapurna–Manaslu region (Central Nepal), *J. Geophys. Res.* 97 (1992) 2107–2128.
- [43] C. Pinet, C. Jaupart, J.C. Mareschal, C. Gariépy, G. Bienfait, R. Lapointe, Heat flow and structure of the lithosphere in the eastern Canadian shield, *J. Geophys. Res.* 96 (1991) 19941–19963.
- [44] R. Bousquet, B. Goffé, P. Henry, X. Le Pichon, C. Chopin, Kinematic, thermal and petrological model of the Central Alps: leopantine metamorphism in the upper crust and eclogitisation of the lower crust, *Tectonophysics* 273 (1997) 105–127.
- [45] B.C. Burchfiel, C. Zhiliang, K.V. Hodges, L. Yuping, L.H. Royden, D. Changrong, X. Jiene, The southern Tibetan detachment system, Himalayan orogen: extension contemporaneous with and parallel to shortening in a collisional mountain belt, *Geological Society of America Special Paper*, vol. 269, 1992, pp. 1–41.
- [46] K. Hodges, Tectonics of the Himalaya and southern Tibet from two perspectives, *GSA Bull.* 112 (3) (2000) 324–350.
- [47] C. Beaumont, R.A. Jamieson, M.H. Nguyen, S. Medvedev, Crustal channel flows: 1. Numerical models with applications to the tectonics of the Himalayan–Tibetan orogen, *J. Geophys. Res.* 109 (2004) B06406, doi:10.1029/2003JB002809.
- [48] R.A. Jamieson, C. Beaumont, S. Medvedev, M.H. Nguyen, Crustal channel flows: 2. Numerical models with implications for metamorphism in the Himalayan–Tibetan orogen, *J. Geophys. Res.* 109 (2004) B06407, doi:10.1029/2003JB002811.
- [49] K. Stuwe, L. White, R. Brown, The influence of eroding topography on steady state isotherms—Application to fission-track analysis, *Earth Planet. Sci. Lett.* 124 (1994) 63–74.
- [50] W.J. Dunlap, G. Hirth, C. Tessier, Thermomechanical evolution of a ductile duplex, *Tectonics* 16 (6) (1997) 983–1000.
- [51] K. Arita, R.D. Dallmeyer, A. Takasu, Tectonothermal evolution of the Lesser Himalaya, Nepal: constraints from  $^{40}\text{Ar}/^{39}\text{Ar}$  ages from the Kathmandu Nappe, *The Island Arc* 6 (1997) 372–385.
- [52] K. Arita, Y. Ganzawa, Thrust tectonics and uplift process of the Nepal Himalaya revealed from fission-track ages (in Japanese with English abstract), *J. Geogr.* 106 (1997) 156–167 (Tokyo Geographical Society).
- [53] A.M. Macfarlane, Chronology of tectonic events in the crystalline core of the Himalaya, Langtang national park, central Nepal, *Tectonics* 12 (1993) 1004–1025.
- [54] W.E. Hames, S.A. Bowring, An empirical evaluation of the argon diffusion geometry in muscovite, *Earth Planet. Sci. Lett.* 124 (1994) 161–167.
- [55] F.D. Hansen, N.L. Carter, Creep of selected crustal rocks at 1000MPa, *Eos Trans. Am. Geophys. Union* 63 (1982) 437.